# Intermolecular interactions drive protein adaptive and co-adaptive evolution at both species and population levels

Junhui Peng, Li Zhao

Laboratory of Evolutionary Genetics and Genomics, The Rockefeller University, New York, NY 10065, USA

*Correspondence to: lzhao@rockefeller.edu

## Abstract

Proteins are the building blocks for almost all the functions in cells. Understanding the molecular evolution of proteins and the forces that shape protein evolution is an essential step in understanding the basis of function and evolution. Previous studies have shown that adaptation occurs frequently at the protein surface, such as in genes involved in host-pathogen interactions. However, it remains unclear whether adaptive sites are distributed randomly or at regions that are associated with particular structural or functional characteristics across the genome, since many of the proteins lack structural or functional annotations. Here, we seek to tackle this question by combining large-scale bioinformatic prediction, structural analysis, phylogenetic inference, and population genomic analysis of *Drosophila* protein-coding genes. By estimating and comparing the rate of adaptive substitutions at protein and residue level, we showed that adaptation is more relevant to function-related rather than structure-related properties. Among the function-related properties, we found that molecular interactions in proteins contribute to adaptive evolution, and putative binding residues exhibit higher rates of adaptation. We observed that physical interactions might play a role in the co-adaptation of fast-adaptive proteins. We found that strongly differentiated amino acids in protein coding genes are mostly adaptive, which may contribute to the long-term adaptive evolution. Our results suggest important roles of intermolecular interactions and co-adaptation in the adaptive evolution of proteins both at the species and population levels.

## Introduction

Natural selection plays an important role in molecular evolution of protein sequences. Recent advances in genome sequencing and reliable inference methods at both phylogenetic and population levels have enabled fast and robust estimation of evolutionary rates and adaptation driven by natural selection. In addition, the increased availabilities of structural and functional data of proteins have made it possible to study how structural and functional constraints affect

protein sequence evolution and adaptation. It is now well established that different proteins and different sites within a protein have varying rates of evolution and adaptation due to both structural and functional constraints (Echave et al., 2016; Kosiol et al., 2008; Lindblad-Toh et al., 2011; Zhang and Yang, 2015). For example, genes that are highly expressed or perform essential functions are under strong purifying selection and tend to evolve slowly (Drummond et al., 2005; Moutinho et al., 2019; Pál et al., 2001; Zhang and He, 2005; Zhang and Yang, 2015); genes involved in host-pathogen interactions, e.g., immune responses and antivirus responses, show exceptionally high rates of adaptive changes (Enard et al., 2016; Nielsen et al., 2005; Obbard et al., 2009; Palmer et al., 2018; Sackton et al., 2007; Sironi et al., 2015; Uricchio et al., 2019); and residues that are intrinsically disordered or at the protein surface are fast evolving and has been proved to be hotspots of adaptive evolution (Afanasyeva et al., 2018; Goldman et al., 1998; Lin et al., 2007; Moutinho et al., 2019; Ramsey et al., 2011). More recently, Slodkowicz & Goldman (Slodkowicz and Goldman, 2020) employed genomic-scale integrated structural and phylogenetic evolutionary analysis in mammals and showed that positively selected residues are clustered near ligand binding sites, especially in proteins that are associated with immune responses and xenobiotic metabolism.

Although evidence have shown that adaptation is more likely to occur at intrinsically disordered regions and clustered at the surface of proteins, the functional properties of adaptation in the genomic scale remains unclear. Moreover, due to lack of structural and functional information of many proteins in the genome, the underlying mechanism derived from current studies might be incomplete. Here, we systematically investigated the evolution and adaptation of protein-coding genes in *Drosophila melanogaster* by comparing it to its closely related species, in order to distinguish the main factors that impact the evolution and adaption at the protein-coding level. We applied large-scale bioinformatic and structural analysis to obtain structural and functional properties of proteins. We then classified residues into different structural and functional sites. By comparing rates of sequence evolution and adaptation between different proteins and different sites, we were able to locate hotspots of adaptation at genome scale. We showed that, for *D. melanogaster* proteins, adaptation is more sensitive to functional properties rather than structural ones. Interestingly, we found that putative binding regions including allosteric sites at protein surface show higher rates of adaptation than other sites. For proteins that are under fast-adaptive evolution, we showed that they tend to interact with each other more frequently than random expectations and are often associated with reproduction, immunity, and environmental information processing in *D. melanogaster*. In addition, we showed that interacting proteins in *D. melanogaster* might undergo co-adaptive

evolution. Furthermore, we hypothesize that molecular interactions or physical interactions might be an important mechanism that contribute to the adaptive and co-adaptive evolution in *D. melanogaster* genome. At last, we showed that the accumulation of short-term adaptation to local environments could be a possible genetic mechanism that contribute to long-term adaptive evolution.

## Results

### Impact of gene properties on evolution of protein-coding genes in *D. melanogaster*

To uncover the main factors that impact the evolutionary rates of genes, we analyzed 13528 protein-coding genes in *D. melanogaster* using genome data from *melanogaster* subgroup species and *D. melanogaster* population genomics data from 205 inbred lines from Drosophila Genetic Reference Panel, Freeze 2.0, DGRP2 (Huang et al., 2014). We applied a maximum likelihood method (Yang, 2007) to compute dN/dS ratio (ω) using the protein-coding sequences of five closely related melanogaster subgroup species (*D. melanogaster*, *D. simulans*, *D. sechellia*, *D. yakuba* and *D. erecta*). We estimated the proportions of adaptive changes (α) in each gene by applying an extension of MK test named asymptotic MK (Messer and Petrov, 2013; Uricchio et al., 2019) using *D. simulans* as outgroup. We then calculated the rate of adaptive changes ($\omega_a$) of each gene by multiplying ω to α ($\omega_a = \alpha\omega$) (Moutinho et al., 2019) using *D. yakuba* as the outgroup species (See methods). The rate of nonadaptive changes can be further calculated by $\omega_{na}=\omega-\omega_a$. Finally, we successfully assigned ω to 12118 protein coding genes and $\omega_a$ and $\omega_{na}$ to 7192 genes.

For each of *D. melanogaster* genes subjecting the same pipeline of analysis, we further obtained 17 different structural or functional properties (see Methods), which can be further divided into two categories: structure-related properties and function-related properties. Specifically, structure-related properties include ratio of secondary structures (helix ratio, sheet ratio, helix+sheet ratio, coil ratio), intrinsic structural disorder (ISD), relative solvent accessibility (RSA); while function-related properties include gene pseudo-age, protein length, number of protein-protein interactions (PPI numbers), ratio of protein-binding sites (PPI-site ratio), ratio of DNA-binding sites (DNA-site ratio) and gene expression patterns such as male expression level, female expression level, mean expression level, male specificity and tissue specificity. The properties along with gene-specific protein evolution (ω, $\omega_a$ and $\omega_{na}$) are available in supplementary file S1.

***Molecular interactions contribute to the variations of protein sequence evolution and adaptation*.** In order to identify the determinants that drive protein evolution (ω, $\omega_a$ and

$\omega_{na}$), we calculated the Pearson's correlations of $\omega$, $\omega_a$ and $\omega_{na}$ with all the structure- and function-related properties. The correlation coefficient (r) and corresponding p-values (p) of each of the properties were listed in Table 1. Interestingly, we observed that for structure-related properties (secondary structure ratios, ISD, and RSA), variation of $\omega$ is dominated by nonadaptive changes ($\omega_{na}$) (Figure S1). Taking RSA as an example, we observed that RSA strongly correlates with both $\omega$ (r=0.16, p=1e-73) and $\omega_{na}$ (r=0.15, p=3e-35), while weakly correlates with $\omega_a$ (r=0.06, p=1e-6). These correlations suggest that, under the constraints of structure-related properties, relaxation of purifying selection may play a more important role in determine protein evolution. These are in line with previous studies that proteins with less structural constraints, i.e. those harboring more disordered, exposed sites display faster evolutionary and nonadaptive evolutionary rate (Afanasyeva et al., 2018; Moutinho et al., 2019)

However, for function-related properties (gene pseudo-age, protein length, PPI number, PPI-site ratio, DNA-site ratio and gene expression patterns), the importance of $\omega_a$ in shaping protein evolution begin to emerge (Figure S1). For example, when considering tissue specificity, the correlation efficient (r) of $\omega$ is 0.30 (p=2e-205), while r of $\omega_a$ and $\omega_{na}$ are 0.16 (p=3e-35) and 0.17 (p=2e-42), respectively. In such cases, the correlations of $\omega_a$ and $\omega_{na}$ almost contributed equally to the variation of protein sequence evolutionary rates, $\omega$. Interestingly, among the function-related properties, we found that molecular interactions, i.e., protein interactions, strongly positively correlates with $\omega$, $\omega_a$ and $\omega_{na}$ (Table 1). We also noticed that for molecular interactions, compared to other function-related properties, variations of $\omega_a$ contributes slightly to variations of $\omega$. This could be a result of intercorrelations of molecular interactions and ISD or RSA (Table S1), since disordered regions and exposed regions are often responsible for interacting with other molecules (Keskin et al., 2008; Van Der Lee et al., 2014). These results highlight the non-neglected contributions of functional constraints, including molecular interactions, on the adaptive evolution of protein-coding sequence.

***Complex correlations of protein length and male expression level with protein evolutionary rates*.** To better clarify and visualize the correlations of $\omega$, $\omega_a$, and $\omega_{na}$ with gene properties in a refined fashion, we divided *D. melanogaster* genes into 15 groups according to the ascending orders of $\omega$ values and compared these properties of different gene groups, while ensuring that each gene group contains the same total number of amino acids (Figure S2). Overall, for most of the properties being investigated, we observed similar correlations as shown in Table 1. For example, fast evolving genes are relatively young, short, lowly expressed, male or tissue specific, abundant of disordered, exposed residues, excluded in protein-protein network center hubs, and abundant of protein and DNA binding sites.

In contrast to previous observations, we found complex (nonlinear) correlations of ω gene groups with protein length and gene expression levels (Figure 1). For protein length, our Pearson correlation analysis (Table 1) and a number of previous studies have suggested a strong negative correlations with ω (Lipman et al., 2002; Moutinho et al., 2019). However, we observed that some proteins with the slowest evolutionary rates, i.e. with the smallest ω values, are significantly shorter than other gene groups with intermediate evolutionary rates (Fig. 1A). These include highly conserved genes such as eIF1A (ω=0.0001,148 a.a), rala (ω=0.0001, 201 a.a.), ctp (ω=0.0001, 89 a.a.), and Mlc-c (ω=0.0001, 153 a.a.).

Similar complex correlations were also observed in male expression level and mean expression level (Fig. 1BC). We found that, when checking male expression level and mean expression level, the gene group that shows the largest mean ω has higher expression than those with intermediate ω. Such U-shape correlations were not observed in female expression levels. Although protein length and mean expression levels of genes are known to be strongly correlated with protein evolutionary rates as listed in Table 1 and also in other references (Drummond et al., 2005; Lipman et al., 2002; Zhang and Yang, 2015), fast evolving genes can also be moderately or highly expressed, especially in male *D. melanogaster*. For example, many seminal fluid proteins show high ω values and are highly expressed, such as Sfp60F (ω=0.77, 82 a.a.), EbpII (ω=0.68, 66 a.a), Acp36DE (ω=0.68, 912 a.a.,), and Dup99B (ω=0.63, 54 a.a.). These proteins evolve at very fast rates (Begun and Lindfors, 2005; Swanson et al., 2001), contain various range of amino acids (54 in Dup99B to 912 in Acp36DE), and are moderately or highly expressed in male *D. melanogaster* (TPM ranging from 440 for Acp36DE to 3189 for Sfp60F), lowly expressed in female (TPM all around 1, presumably in spermatheca). We listed all the genes and protein length and expression levels in each ω gene group, which can be found in supplementary file S2.

Since tissue specificity and male specificity both strongly correlates with ω, $\omega_a$, and $\omega_{na}$ (Table 1), we asked whether male specificity would be a redundant property compared to tissue specificity to indicate protein evolution due to the complex correlations of male expression levels. To answer this question, we classified *D. melanogaster* genes into 15 groups according to ascending values of male specificity. We then did similar classification to classify all the genes into 15 groups according to ascending values of tissue specificity (Figure 1). As expected, we found that tissue specificity positively correlates with ω, $\omega_a$ and $\omega_{na}$ (Fig. S3). However, we observed complex correlations for male specificity gene groups. Specifically, gene group with the lowest male specificity show significantly higher ω, $\omega_a$ and $\omega_{na}$ than its following

gene group (Fig. S3). This could be a result of fast evolving female-biased genes (Yang et al., 2016) included in this gene group.

**Putative molecular interaction sites are hotspots for protein adaptive evolution**

Having established that molecular interactions positively correlates with the adaptation of protein sequence, we next investigate whether residues involved in molecular interactions are targets for adaptive evolution. To tackle this question, we predicted protein-protein interaction sites (PPI-sites) and DNA binding sites (DNA-sites) for each of *D. melanogaster* protein sequence (see Methods). In addition, we characterized allosteric residues as surface and interior critical residues with STRESS model (Clarke et al., 2016) for all the structural models. We also extracted putative binding sites from STRESS Monte Carlo (MC) simulations. We calculated $\omega$, $\omega_a$ and $\omega_{na}$ for residues in each of the putative molecular interaction category. Strikingly, we observed that residues involved in protein-protein interactions, DNA binding and ligand binding exhibited higher rates of adaptive evolution compared to their corresponding null sites (Fig. 2A-C). In addition, allosteric residues at protein surface showed higher adaptation rates than allosteric residues at protein interior or residues that are not involved in ligand binding from STRESS simulations (Fig. 2C).

Since we observed significant positive intercorrelations between PPI and DNA binding with ISD and RSA (Table S1), we next asked whether the increase of $\omega_a$ in protein-protein interactions sites or DNA binding sites was caused by the increase of disorder or site exposure. We calculated and compared $\omega$, $\omega_a$ and $\omega_{na}$ for putative PPI and DNA binding sites with different levels of ISD or RSA. Remarkably, we found that $\omega_a$ of these putative binding sites remains similar among different levels of ISD or RSA (Fig. S4, left column). The results suggest that putative PPI or DNA binding events in proteins can result in elevated adaptation rates regardless their structural disorder or site exposure. While for residues that are not associated with putative PPI or DNA binding, we also observed increase in $\omega_a$ when increasing ISD or RSA (Fig. S4, right column), which could be the result of some other yet unknown underlying mechanisms or inaccuracy of putative binding sites predictions.

In order to gain better understanding of adaptation in molecular interaction sites, we further visualized positive selections that are associated with molecular interactions. We first investigated whether adaptive evolution is associated with particular protein structures or protein families. To do this, we looked into fast-adaptive proteins with the largest ~15% rates of adaptation ($\omega_a > 0.15$) that are linked to high quality structural models. Interestingly, among these proteins, we found 45 enriched as trypsin-like cysteine/serine peptidase domain and 17

7TM chemoreceptors, suggesting widespread adaptive evolution acting on these protein families or protein domains in *D. melanogaster* (Table S2). Many of the 7TM chemoreceptors are olfactory and gustatory genes, which shows adaptive evolution in various species such as *Drosophila* and mosquito (Hill et al., 2002; Lawniczak and Begun, 2007; McBride, 2007; Wu et al., 2009). In addition to these two protein families, recurrent positive selections acting on some other fast-adaptive proteins were identified in previous studies in *Drosophila* and mammals, and the possible adaptive evolution mechanisms have been linked to exogenous ligand binding, for example, serine protease inhibitors (serpin), Toll-like receptor 4 (TLR-4), and cytochrome P450 (Jiggins and Kim, 2007; Slodkowicz and Goldman, 2020).

In order to visualize the link between adaptive evolution and molecular interactions in the two protein families with frequent adaptive evolution, we showed significant positive selections and molecular interactions in two representatives: CG10232 and Or67a, each for trypsin-like cysteine/serine peptidase domain and 7TM chemoreceptors, respectively. We observed that in both cases, positively selected sites highly overlapped with predicted or inferred binding pockets (Fig. 2D-E). Specifically, in CG10232, we found clusters of positive selected sites around NAG binding sites that are inferred from a crystal structure of serine protease (PDB code: 2XXL) (Fig. 2D), while in Or67a, positively selected sites expand around the putative odorant binding channel formed by helices S1-S6 in extracellular regions (Butterwick et al., 2018) (Fig. 2E).

Except for these examples that are associated with exogenous ligand or exogenous peptide binding, we also identified two previously not described examples where adaptive evolution might be linked to endogenous protein binding: Spaztle (spz, Fig. 2F) and Cul6 (Fig. 2G). Spaztle can bind to Toll-like receptors (TLR) and trigger humoral innate immune response. We built the missing loop in Spaztle in the crystal structure of Toll/Spaztle complex (PDB code 4BV4) according to the dimeric crystal structure of Spaztle (PDB code 3E07). In this complex structural model, we observed several positively selected sites in Toll-4/Spaztle interfaces (Fig. 2F). Cul6, another example, is a protein in cullins family in *D. melanogaster*. The cullins protein family are known as scaffold proteins that assemble multi-subunit Cullin-RING E3 ubiquitin ligase by forming SCF complex with F box and RING-box (Rbx) proteins (Zheng et al., 2002). We constructed the putative Cul6 contained SCF complex by superimposition to the crystal structure of the Cul1-Rbx1-Skp1-F box$^{Skp2}$ SCF ubiquitin ligase complex (Zheng et al., 2002). In the structural model, we observed positive selected sites in Cul6 clustered around the binding sites of RING-box protein, Rbx1, and F-box protein, Skp1 (Fig. 2G).

**Frequent adaptive evolution and co-adaptative evolution in genes involved in reproduction, immune system and environmental information processing**

To find out whether specific biological functions were associated with fast-adaptive genes, we applied DAVID Go analysis with genes that have largest ~15% rates of adaptation ($\omega_a > 0.15$). The significant Go terms are frequently linked to serine-type endopeptidase activity, reproduction, protein lysis, chemosensory and other related biological functions (Table S3). As these fast-adaptive genes tend to be enriched in similar biological functions, we asked whether these genes are evolved co-adaptively, i.e., whether these proteins are interacting with each other frequently. To test this possibility, we obtained PPI of *D. melanogaster* from STRING database (Szklarczyk et al., 2019) and analyzed protein-protein interactions among fast-adaptive proteins. We found that fast-adaptive proteins tend to interact with each other more frequently than expected (PPI enrichment p-value < 1.0e-16). In the PPI network of fast-adaptive proteins, we observed 7 strongly connected sub-clusters with at least 5 members (Fig. 3A, Table S4). Proteins in these sub-clusters are enriched in biological processes such as reproduction, immune response, defense response to bacterium and virus, RNA interference, chitin metabolic, etc., which are in line with the Go analysis of fast-adaptive genes (Table S5-S10).

We next asked whether co-adaptation plays a role in the adaptive evolution of interacting proteins to a broader extend, including both fast- and slow-adaptive proteins. To address this question, we analyzed and compared adaptation rates of all PPIs available in STRING database with high confidence in *D. melanogaster* and we found that protein partners of fast-adaptive proteins ($\omega_a>0.15$) have significantly larger maximum/average $\omega_a$ compared to slow-adaptive proteins (Figure 4). We further analyzed and visualized adaptive evolutionary rates of proteins in PPI networks of 9 different biological pathways extracted from KEGG pathways, including immune system, xenobiotics biodegradation, response to environment, aging and development, genetic information processing, sensory system, transport and catabolism, cell growth and death and metabolism. We observed that, in these PPI networks, proteins with relatively large $\omega_a$ tend to interact with each other (Figure S5A, S5B). We also noticed that, for pathways that are previously known as adaptation-hotspots, e.g., immune system, fast-adaptive proteins can act as central nodes and are co-adaptively evolved with other fast-adaptive proteins (Figure S5C). While in pathways such as transport and catabolism, fast-adaptive proteins are mainly at PPI periphery. In line with these findings, we found that $\omega_a$ are larger in pathways that harbor fast-adaptive proteins as central nodes than other pathways (Figure S6).

***Physical interactions contribute to co-adaptation of fast-adaptive genes.*** Having established that molecular interactions contribute to adaptive evolution of protein sequence, we then investigated whether these physical molecular interactions could drive protein-protein co-adaptation. To do this, we looked into interacting fast-adaptive protein pairs that are associated known or inferred complex structural models. For inferred complex structural models, we superimposed the structural models of the pair of proteins onto their high resolution homologous complex structures. Here we observed and illustrated co-adaptation at PPI interface in two examples: Toll-4/Spatzle and Spn28Db/CG18563 (Figure 3).

***Toll-4/Spatzle***. Toll-4 is a member of toll-like receptors. Previous studies have shown strong evidence of adaptive evolution of Toll-4 in *Drosophila* and mammals (Levin and Malik, 2017; Slodkowicz and Goldman, 2020). Toll-4 can bind to Spatzle and trigger further innate immune responses with high confidence (inferred from STRING database). In the previous section, we showed that several positively selected sites in Spatzle overlap with Toll-Spatzle interfaces. Here, we further showed that, in Toll-4, considerable number of significant positively selected sites were located at interface for Spatzle (Fig. 3B), which is in line with a previous study of Toll-4 in *D. willistoni* (Levin and Malik, 2017).

***Spn28Db/CG18563***. Spn28Db is one of the serine protease inhibitors in *D. melanogaster* that are expressed in male accessory glands, while CG18563 belongs to the protein family of trypsin-like cysteine/serine peptidase domain. The interactions between the two proteins were predicted with high confidence from STRING database, and the molecular interactions can be inferred from existing crystal structure of serpin and bacteria protease complex (PDB code 1EZX). We observed many positive selected sites at the molecular interface between the two proteins (Fig. 3C), suggesting that physical interactions might play a role in the co-adaptation of the two proteins.

**Most clinally differentiated SNPs in protein-coding genes are adaptive**

To find out the relations between short-term adaptation to local environments and long-term adaptive evolution, we extracted residues with significant $F_{ST}$ SNPs from clinal variations (Svetec et al., 2016). We then computed evolutionary rates (ω), adaptation rates ($\omega_a$) and non-adaptation rates ($\omega_{na}$) of these residues as in previous section. We observed that these residues have much higher ratio of adaptation rates over non-adaptation rates than genome-wide random expectations (Figure 5), suggesting that these residues have higher proportions of adaptive changes, and that they can be hotspots for adaptive evolution. To further characterize structural and functional properties of short-term genetic variations, we mapped significant

303 nonsynonymous $F_{ST}$ residues to different structural and functional characteristics, such as ISD,
304 RSA, PPI-sites, DNA-sites and ligand-binding sites. We found that these nonsynonymous SNPs
305 follow the patterns of adaptive changes. For example, they were enriched disordered regions
306 and protein surfaces, and were significantly more likely to be involved in protein-protein
307 interactions and ligand-binding than expectation (Table S11-S15).
308
309 **Discussion**
310 In this study, we systematically studied the impact of structure- and function-related gene
311 properties on protein sequence evolution and adaptation in *D. melanogaster* genome. We found
312 that, compared to protein structure-related properties, such as intrinsic structural disorder (ISD)
313 and relative solvent accessibility (RSA), function-related properties, such as tissue specificity
314 and male specificity, contribute more extensively to protein sequence adaptive evolution.
315 Especially, we noticed that molecular interactions in proteins contribute to the variation of
316 protein sequence adaptive evolution. In line with this result, we detected that molecular
317 interaction sites are hotspots for adaptative evolution. We confirmed that proteins that are fast
318 adaptive are enriched in GO terms that are associated reproduction, immunity and
319 environmental information processing. Furthermore, we revealed that fast-adaptive proteins
320 tend to interact with each other frequently and protein partners of these fast-adaptive proteins
321 tend to have higher adaptation rates, suggesting that co-adaptive evolution might be common in
322 *D. melanogaster*. By looking at interacting fast-adaptive proteins, we further demonstrated that
323 physical interactions may contribute to the mechanisms of co-adaptative evolution of fast-
324 adaptive proteins.
325 Extensive studies have been conducted to uncover the main drivers that govern protein
326 sequence evolutionary rate (Zhang and Yang, 2015). Gene expression level was proved to be a
327 major determinant (Zhang and Yang, 2015) through mechanisms such as the pressure for
328 translational robustness, i.e., robustness to translational missense errors (Drummond et al.,
329 2005). Here, we showed that caveat exists when we looked at gene expression levels in male
330 *D. melanogaster*. Previous studies have revealed that male biased or female biased genes can
331 be fast evolving (Yang et al., 2016). On the other hand, many male biased genes can be highly
332 expressed in testis, which results in a complex correlation between protein sequence
333 evolutionary rate and male expression level or even mean expression level of *D. melanogaster*.
334 The unique evolutionary property of these male biased or specific genes could be caused by the
335 unique transcriptional scanning mechanism in testis (Xia et al., 2020). We propose that tissue
336 specificity might be a better quantity when considering the impact of gene expression profile on

protein sequence evolution in *D. melanogaster*. In addition to male expression level, a similar complex correlation was observed for protein length. It has been the notion that short proteins tend to evolve faster than long proteins, which may be biologically relevant or byproduct of other factors such as selection on buried and exposed sites (Moutinho et al., 2019). Here, we demonstrated that, in *D. melanogaster*, although protein length is strongly negatively correlated with protein sequence evolutionary rate, genes that have the slowest evolutionary rates tend to be relatively short. This could be caused by the fact that under essential functional constraint, genes can undergo strong purifying selections, while essential genes such as secreted proteins are constrained to be smaller, and that essential genes could be shorter than other genes (Chen et al., 2020).

It has been recognized that protein surface and intrinsic disorder regions are frequent targets for adaptive evolution and contribute to the variations of protein sequence adaptive evolution (Afanasyeva et al., 2018; Moutinho et al., 2019). However, the detailed mechanisms underlying these observations remains unclear. One possible explanation would be that these regions are frequently linked to intermolecular interactions (Afanasyeva et al., 2018; Moutinho et al., 2019). For example, Moutinho et al hypothesized that molecular interactions involved in host-pathogen coevolution were the major driver of protein adaptation (Moutinho et al., 2019). Here, we further identified that proportions of possible molecular interaction sites inside proteins contribute to the variations of protein sequence adaptive evolution and that these molecular interaction sites or regulatory sites at protein surface can be hotspots of protein adaptation. Indeed, some specific molecular interactions have been linked to adaptive evolution in several case studies (Bachtrog, 2008; Hughes and Nei, 1988; Levin and Malik, 2017; Schott et al., 2014) and large-scale studies based on proteins with high quality structural models (Slodkowicz and Goldman, 2020). In the latter study, the authors showed that positive selections in mammals tend to cluster closer to binding sites of exogenous ligands than expected by chance (Slodkowicz and Goldman, 2020), suggesting an important role of function important regions in adaptive evolution. Here, we extend the conclusion *to D. melanogaster* genome, including proteins with or without high resolution structural models. We also showed that except for exogenous ligands, endogenous ligands might also contribution to adaptive evolution, while the latter might explain why interacting proteins tend to evolve co-adaptively.

Notably, previous studies have revealed that multi-interface proteins tend to be evolving more slowly than single-interface proteins (Kim et al., 2006), which seems to be contradictory to our results that proteins with more interaction sites evolve faster and have faster adaptation rates. Here, we argue that, in our study, we used sequence profile to predict molecular

interaction sites in proteins at a genomic scale, rather than only looking into proteins with high resolution structures. In this way, we may capture many weak or transient interactions, which are thought to be evolving faster than obligate and conserved interactions (Mintseris and Weng, 2005). Meanwhile, we did not exclude intrinsic disordered regions (IDR) or intrinsic disordered proteins (IDP) in our study, which are widespread in *D. melanogaster* genome. It has been suggested that IDR/IDP tend to evolve fast due to lack of structural restraints (Echave et al., 2016). In the functional aspect, IDR/IDP are thought to be promiscuous binders through many multiple binding mechanisms, including forming static, semi-static, and fuzzy or dynamic complexes (Uversky, 2019), suggesting that the evolution of IDR/IDP cannot be explained merely by the lack of structural restraints. Actually, IDP and IDR in human genome were found to be undergoing extensive adaptive evolution (Afanasyeva et al., 2018). At last, it has been recognized that, except for allosteric regulations, encounter complexes (Gabdoulline and Wade, 1999) might also play an important role in mediating intermolecular interactions, such as protein-protein association (Tang et al., 2006) and protein-ligand binding (Re et al., 2019). Since encounter residues that are responsible for encounter complexes do not reside in conserved binding interfaces, these residues could be under relaxed purifying selections or even positive selections, which could be another yet-to-identify mechanism that contribute to protein sequence adaptive evolution.

In consistent with previous studies in *D. melanogaster* (Begun and Lindfors, 2005; Begun and Whitley, 2000; Lazzaro et al., 2004), we showed that fast-adaptive proteins are enriched in molecular functions such as reproduction, immunity and environmental information processing. We further demonstrated that fast-adaptive proteins tend to interact with each other more frequently than random expectations, suggesting co-adaptation might be common among fast-adaptive proteins. Mechanisms that contribute to the co-adaptation could be: (1) interacting fast-adaptive proteins are often enriched in similar molecular functions and under similar selective pressure; (2) interacting fast-adaptive undergo co-evolution through physical interactions. In this study we showed two examples that adaptive evolution could occur at protein-protein interface, which suggest that physical interactions could contribute to the co-adaptation of fast-adaptive proteins in *D. melanogaster*. Moreover, we showed that co-adaptation might exist to a broader extend rather than only among fast-adaptive proteins. Specifically, proteins that interact with fast-adaptive proteins tend to have higher adaptation rates. Since molecular interactions contribute to adaptive evolution, it is reasonable to hypothesize that co-adaptation at this broader extend could be regulated by these interactions. Actually, it has been suggested that interacting proteins tend to have similar evolutionary rates

and the possible mechanism would be the co-evolution of physical interactions (Pazos and Valencia, 2008).

It has been suggested that populations in different local environments can have genetic variances that result in local adaptations. In this study, we found that loci with significant genetic variance among populations harbor higher proportions of long-term adaptive changes and these loci follow similar patterns as adaptive changes, i.e. they are enriched in disordered regions, protein surfaces, and functionally important regions. These results suggest that population differentiation of protein-coding genes can be an important basis for long-term adaptive evolution. Importantly, our results indicate that most of the clinal amino-acid changes are adaptive, suggesting that non-selective forces play a non-essential role in the SNPs that show strong geographic differences. Our results also support a large effect of spatially varying selection on protein sequence and structures (Storz and Kelly, 2008).

It should be noted that studies at the genomic scale that aim to uncover the function- or structure-related constraints imposed on protein sequence evolution and adaptation share similar limitations that for most of the proteins or residues, structural or functional information would be incomplete or even missing. Thus, in this study, we used highly accurate neural-network based tools to predict molecular interactions, secondary structures, intrinsic structural disorder, relative solvent accessibility for each of the protein in *D. melanogaster* genome. In this way we were able to identify key factors that impact protein sequence evolution and adaptation in a less accurate but rather systematic fashion. We hope that with the availability of more and more curated structural, functional information and complex structural models of proteins in the near future, we will be able to uncover the precise role of molecular interactions in protein sequence adaptive evolution.

## Material and Methods

***$d_N/d_S$* ratio (ω).** We used a maximum likelihood method to infer $d_N/d_S$ ratio (ω) of *D. melanogaster* protein-coding genes using the genome sequences of five species in *melanogaster* subgroup (*D. melanogaster*, *D. simulans*, *D. sechellia*, *D. yakuba*, and *D. erecta*). The protein-coding sequences were extracted from the alignments of 26 insects, which were obtained from UCSC Genome Browser (http://hgdownload.soe.ucsc.edu/downloads.html). The sequences were further processed by GeneWise (Birney et al., 2004) to remove possible insertions and deletions using the longest isoforms of the corresponding *D. melanogaster* protein sequences as references (FlyBase version r6.15) (Thurmond et al., 2019). The processed sequences were then realigned by PRANK -codon function (Löytynoja, 2014). We

used codeml in PAML (Yang, 2007) to compute gene-specific ω using M0 model. We removed sequences that have more than 15% of their nucleotides not aligned (gaps) to *D. melanogaster* genes in more than 2 species. To further avoid numeric errors and ensure reasonable estimations, we only retained relatively divergent sequences that are: (1) divergent with dS larger than 0.3, (2) less divergent with dS larger than 0.1 and dN smaller than 0.001 (dS>>dN). At last, there were 12118 genes in total passed all the criteria and were assigned gene specific ω, containing 6,538,872 amino acids. We also calculated site-specific ω by using likelihood ratio tests (LRT) comparing M7 model against M8 model (Yang et al., 2005).

***Rate of adaptive and nonadaptive changes.*** We recalled all SNPs of 205 inbred lines from the Drosophila Genetic Reference Panel (DGRP), Freeze 2.0 (Huang et al., 2014) (http://dgrp2.gnets.ncsu.edu). We then generated 410 alternative genomes using all monoallelic and bi-allelic SNP data sets. We extracted the coding sequences of *D. melanogaster* genes from the generated alternative genomes, removed all possible insertions and deletions using GeneWise (Birney et al., 2004) as described above. We then align all the coding sequences to their corresponding aligned CDS sequences using PRANK -codon function (Löytynoja, 2014). We removed polymorphisms segregating at frequencies smaller than 5% to reduce possible slightly deleterious mutations (Charlesworth and Eyre-Walker, 2008). In order to avoid possible effects of low divergence between *D. simulans* and D melanogaster (Keightley and Eyre-Walker, 2012), we used *D. yakuba* as outgroup to estimate nonsynonymous polymorphisms (Pn), synonymous polymorphisms (Ps), nonsynonymous substitutions (Dn) and synonymous substitutions (Ds) by MK.pl (Begun et al., 2007; Langley et al., 2012). Similar as Begun et al. (Begun et al., 2007), we only analyzed genes with at least six variants for each of substitutions, polymorphisms, nonsynonymous changes and synonymous changes. We used an extension of MK test, asymptotic MK (Messer and Petrov, 2013; Uricchio et al., 2019), to estimate the proportions of adaptive changes (α). The rate of adaptive changes ($\omega_a$) was then calculated as $\omega_a = \omega\alpha$ and the rate of non-adaptive changes as $\omega_{na} = \omega - \omega_a$. Details of the asymptotic MK test were as following:

(1) Classical McDonald–Kreitman test. According to Smith and Eyre-Walker (Smith and Eyre-Walker, 2002), the proportions of adaptive changes for protein-coding genes can be calculated as following:

$$\alpha = 1 - \frac{DsPn}{DnPs}$$

According to this equation, we could estimate the proportion of adaptive changes and carried out classical MK test by applying Fisher's exact test.

(2) Asymptotic estimation of α. A known problem of the classical estimation of α above is the accumulation of slightly deleterious mutations at low frequencies. We therefore used an extension of MK test, asymptotic MK test approach (Messer and Petrov, 2013) to estimate the proportions of adaptive changes. As in original aMK, we defined α(x) as a function of derived allele frequency (x):

$$\alpha(x) = 1 - \frac{DsPn(x)}{DnPs(x)}$$

where Pn(x) and Ps(x) are number of non-synonymous and synonymous polymorphisms at frequency x, respectively. However, the original approach may suffer from numeric errors when there were very few polymorphic sites, which is quite common in many of *D. melanogaster* genes. To make the estimations more robust while preserving the same asymptote, we further define Pn (x) and Ps(x) as total number of Pn and Ps above frequency x as described in Uricchio et al (Uricchio et al., 2019). We fitted α(x) to an exponential curve of $\alpha(x) \approx \exp(-bx)+c$ using lmfit (Newville et al., 2014) and determined the asymptotic value of α at the limit of x, 1.0. We then estimate the rate of adaptive changes ($\omega_a$) as

$$\omega_a = \frac{N_a/L_N}{dS} = \frac{dN_a}{dS} = \frac{dN_a}{dN} \cdot \frac{dN}{dS} = \alpha\omega$$

where $N_a$ is the number of adaptive changes and $dN_a=N_a/L_N$ is the number of adaptive changes per nonsynonymous site. Finally, we calculated the rate of nonadaptive changes ($\omega_{na}$) as $\omega_{na}=\omega-\omega_a$. The final dataset contains 7192 protein-coding genes, with smallest $\omega_a$ being 0.00 and largest being 1.29.

***Structure-/function- related properties of D. melanogaster proteins.*** We obtained function-related properties mentioned in main text as following. We derived *D. melanogaster* gene ages (Kondo et al., 2017; Zhang et al., 2010) for genes that are specific to *Drosophila*, and from GenTree (Shao et al., 2019) for genes that are beyond *Drosophila* clade. We then assigned a pseudo-age to each of the genes. Specifically, there are 11 age groups from “cellular organisms”, assigning to a pseudo age value of 0, to “melanogaster”, assigning a pseudo age value of 10. We downloaded *D. melanogaster* protein-protein interaction (PPI) from STRING database (Szklarczyk et al., 2019). A cut-off of combined score larger than 0.7 was used to retain high confident PPI for further analysis. We then used BSpred (Mukherjee and Zhang, 2011) to predict protein-protein interaction (PPI) sites and DRNApred (Yan and Kurgan, 2017) to predict DNA binding sites. For each protein, we calculated ratios of protein interaction residues (PPI-site ratio) and ratios of DNA binding residues (DNA-site ratio) by dividing total predicted protein interaction sites and DNA binding sites over protein length, respectively. For structure-related properties, we used DeepCNF (Wang et al., 2016) to predict these properties

for each gene, including three-state secondary structures (helix, sheet, and coil), structural disorder, relative solvent accessibility (RSA). Further, we calculated the ratios of helix, sheet, helix+sheet, and coil residues of each gene from predicted secondary structures. For each gene, we computed intrinsic structural disorder (ISD) and relative solvent accessibility (RSA), as protein-length normalized summations of the probabilities of each residue being disorder and exposed, respectively.

***Gene expression patterns*.** We downloaded gene expression profile from FlyAtlas2 (Leader et al., 2018). We converted FPKM to TPM by normalizing FPKM against the summation of all FPKMs as following:

$$\mathrm{TPM_i} = \frac{\mathrm{FPKM_i}}{\sum \mathrm{FPKM_j}} \times 10^6$$

After TPM conversion, we only retained genes with expression level larger than 0.1 TPM for further analysis. We treated male and female whole-body TPM as male and female expression levels. We calculated mean expression level by averaging male and female TPM. We used following Z-score to describe male specificities of *D. melanogaster* genes:

$$zscore = \frac{TPM(male\ expression) - TPM(female\ expression)}{\sqrt{sd^2(male\ expression) + sd^2(female\ expression)}}$$

We calculated tissue specificities of genes using tau values (Yanai et al., 2005) based on the expression profiles of 27 different tissues.

***High quality 3D structures of D. melanogaster proteins.*** We downloaded high-quality structures or structural models of *D. melanogaster* proteins from protein data bank (PDB) (Burley et al., 2019), SWISS-MODEL Repository (Bienert et al., 2017), and MODBASE (Pieper et al., 2011), with descending priorities. For example, if there were 3D structures of a same protein or protein region in multiple databases, we first considered high-resolution structures from PDB; if no structures were found in PDB, we then considered SWISS-MODEL Repository; and at last from MODBASE. In addition, we used blastp (Camacho et al., 2009) to search homologs of each *D. melanogaster* protein against all PDB sequences with E-value threshold of 0.001. We further carried out comparative structural modeling using RosettaCM (Song et al., 2013) to model high-quality structural models of proteins or protein regions that were not available in PDB, SWISS-MODEL Repository and MODBASE. For each RosettaCM simulation, we used no more than 5 most significant hits from blastp search. For proteins that are in complex forms, we only extracted monomers for further analysis. At last, we obtained 14543

high quality structural models, corresponding to 11284 genes. These structural models contain 2,691,913 unique amino acids, 41.2% of all the residues in genes that were assigned ω.

***Evolutionary rates of different structural/functional sites*.** We classified amino acids into different classes of structural/functional properties. Specifically, we classified three classes for both ISD and RSA according the probability of residues being disordered or exposed: ordered or buried (0.00 to 0.33), medium (0.33 to 0.67), disordered or exposed (0.67 to 1.00). For both PPI and DNA binding, we classified two classes: PPI-site or DNA-site (binding sites), None-PPI or None-DNA (corresponding null sites for PPI or DNA binding). For residues that have 3D structures, we used STRESS (Clarke et al., 2016) to predict putative ligand binding sites and allosteric sites from all the high-quality structures or structural models. The allosteric sites were further classified as surface critical or interior critical according to their locations. We then classified these residues into four groups: LIG (ligand binding sites), Surf. Crit. (surface critical sites), Interior Crit. (interior critical sites) and Others (other sites). For each of the site classes, we randomly sampled 1,00 sequences, each containing 10,000 amino acids. We computed ω, $\omega_a$, and $\omega_{na}$ for the randomly sampled sequences similar as the steps described in the above sections.

**Reference**

Afanasyeva, A., Bockwoldt, M., Cooney, C.R., Heiland, I., and Gossmann, T.I. (2018). Human long intrinsically disordered protein regions are frequent targets of positive selection. Genome Res. *28*, 975–982.

Bachtrog, D. (2008). Positive selection at the binding sites of the male-specific lethal complex involved in dosage compensation in Drosophila. Genetics *180*, 1123–1129.

Begun, D.J., and Lindfors, H.A. (2005). Rapid evolution of genomic Acp complement in the melanogaster subgroup of Drosophila. Mol. Biol. Evol. *22*, 2010–2021.

Begun, D.J., and Whitley, P. (2000). Adaptive evolution of relish, a Drosophila NF-kappaB/IkappaB protein. Genetics *154*, 1231–1238.

Begun, D.J., Holloway, A.K., Stevens, K., Hillier, L.W., Poh, Y.-P., Hahn, M.W., Nista, P.M., Jones, C.D., Kern, A.D., Dewey, C.N., et al. (2007). Population Genomics: Whole-Genome Analysis of Polymorphism and Divergence in Drosophila simulans. PLoS Biol. *5*, e310.

Bienert, S., Waterhouse, A., De Beer, T.A.P., Tauriello, G., Studer, G., Bordoli, L., and Schwede, T. (2017). The SWISS-MODEL Repository-new features and functionality. Nucleic Acids Res. *45*, D313–D319.

Birney, E., Clamp, M., and Durbin, R. (2004). GeneWise and Genomewise. Genome Res. *14*,

988–995.

Burley, S.K., Berman, H.M., Bhikadiya, C., Bi, C., Chen, L., Di Costanzo, L., Christie, C., Dalenberg, K., Duarte, J.M., Dutta, S., et al. (2019). RCSB Protein Data Bank: Biological macromolecular structures enabling research and education in fundamental biology, biomedicine, biotechnology and energy. Nucleic Acids Res. *47*, D464–D474.

Butterwick, J.A., del Mármol, J., Kim, K.H., Kahlson, M.A., Rogow, J.A., Walz, T., and Ruta, V. (2018). Cryo-EM structure of the insect olfactory receptor Orco. Nature *560*, 447–452.

Camacho, C., Coulouris, G., Avagyan, V., Ma, N., Papadopoulos, J., Bealer, K., and Madden, T.L. (2009). BLAST+: architecture and applications. BMC Bioinformatics *10*, 421.

Charlesworth, J., and Eyre-Walker, A. (2008). The McDonald-Kreitman test and slightly deleterious mutations. Mol. Biol. Evol. *25*, 1007–1015.

Chen, H., Zhang, Z., Jiang, S., Li, R., Li, W., Zhao, C., Hong, H., Huang, X., Li, H., and Bo, X. (2020). New insights on human essential genes based on integrated analysis and the construction of the HEGIAP web-based platform. Brief. Bioinform. *21*, 1397–1410.

Clarke, D., Sethi, A., Li, S., Kumar, S., Chang, R.W.F., Chen, J., and Gerstein, M. (2016). Identifying Allosteric Hotspots with Dynamics: Application to Inter- and Intra-species Conservation. Structure *24*, 826–837.

Drummond, D.A., Bloom, J.D., Adami, C., Wilke, C.O., and Arnold, F.H. (2005). Why highly expressed proteins evolve slowly. Proc. Natl. Acad. Sci. U. S. A. *102*, 14338–14343.

Echave, J., Spielman, S.J., and Wilke, C.O. (2016). Causes of evolutionary rate variation among protein sites. Nat. Rev. Genet. *17*, 109–121.

Enard, D., Cai, L., Gwennap, C., and Petrov, D.A. (2016). Viruses are a dominant driver of protein adaptation in mammals. Elife *5*, e12469.

Gabdoulline, R.R., and Wade, R.C. (1999). On the protein-protein diffusional encounter complex. J. Mol. Recognit. *12*, 226–234.

Goldman, N., Thorne, J.L., and Jones, D.T. (1998). Assessing the impact of secondary structure and solvent accessibility on protein evolution. Genetics *149*, 445–458.

Hill, C.A., Fox, A.N., Pitts, R.J., Kent, L.B., Tan, P.L., Chrystal, M.A., Cravchik, A., Collins, F.H., Robertson, H.M., and Zwiebel, L.J. (2002). G Protein-Coupled Receptors in Anopheles gambiae. Science (80-. ). *298*, 176–178.

Huang, W., Massouras, A., Inoue, Y., Peiffer, J., Ràmia, M., Tarone, A.M., Turlapati, L., Zichner, T., Zhu, D., Lyman, R.F., et al. (2014). Natural variation in genome architecture among 205 Drosophila melanogaster Genetic Reference Panel lines. Genome Res. *24*, 1193–1208.

Hughes, A.L., and Nei, M. (1988). Pattern of nucleotide substitution at major histocompatibility

603 complex class I loci reveals overdominant selection. Nature *335*, 167–170.
604 Jiggins, F.M., and Kim, K.W. (2007). A screen for immunity genes evolving under positive
605 selection in Drosophila. J. Evol. Biol. *20*, 965–970.
606 Keightley, P.D., and Eyre-Walker, A. (2012). Estimating the rate of adaptive molecular evolution
607 when the evolutionary divergence between species is small. J. Mol. Evol. *74*, 61–68.
608 Keskin, O., Gursoy, A., Ma, B., and Nussinov, R. (2008). Principles of protein-protein
609 interactions: What are the preferred ways for proteins to interact? Chem. Rev. *108*, 1225–1244.
610 Kim, P.M., Lu, L.J., Xia, Y., and Gerstein, M.B. (2006). Relating three-dimensional structures to
611 protein networks provides evolutionary insights. Science (80-. ). *314*, 1938–1941.
612 Kondo, S., Vedanayagam, J., Mohammed, J., Eizadshenass, S., Kan, L., Pang, N., Aradhya, R.,
613 Siepel, A., Steinhauer, J., and Lai, E.C. (2017). New genes often acquire male- specific
614 functions but rarely become essential in Drosophila. 1841–1846.
615 Kosiol, C., Vinař, T., da Fonseca, R.R., Hubisz, M.J., Bustamante, C.D., Nielsen, R., and Siepel,
616 A. (2008). Patterns of Positive Selection in Six Mammalian Genomes. PLoS Genet. *4*,
617 e1000144.
618 Langley, C.H., Stevens, K., Cardeno, C., Lee, Y.C.G., Schrider, D.R., Pool, J.E., Langley, S.A.,
619 Suarez, C., Corbett-Detig, R.B., Kolaczkowski, B., et al. (2012). Genomic variation in natural
620 populations of Drosophila melanogaster. Genetics *192*, 533–598.
621 Lawniczak, M.K.N., and Begun, D.J. (2007). Molecular population genetics of female-expressed
622 mating-induced serine proteases in Drosophila melanogaster. Mol. Biol. Evol. *24*, 1944–1951.
623 Lazzaro, B.P., Sceurman, B.K., and Clark, A.G. (2004). Genetic basis of natural variation in D.
624 melanogaster antibacterial immunity. Science *303*, 1873–1876.
625 Leader, D.P., Krause, S.A., Pandit, A., Davies, S.A., and Dow, J.A.T. (2018). FlyAtlas 2: A new
626 version of the Drosophila melanogaster expression atlas with RNA-Seq, miRNA-Seq and sex-
627 specific data. Nucleic Acids Res. *46*, D809–D815.
628 Van Der Lee, R., Buljan, M., Lang, B., Weatheritt, R.J., Daughdrill, G.W., Dunker, A.K.,
629 Fuxreiter, M., Gough, J., Gsponer, J., Jones, D.T., et al. (2014). Classification of intrinsically
630 disordered regions and proteins. Chem. Rev. *114*, 6589–6631.
631 Levin, T.C., and Malik, H.S. (2017). Rapidly evolving Toll-3/4 genes encode male-specific Toll-
632 like receptors in drosophila. Mol. Biol. Evol. *34*, 2307–2323.
633 Lin, Y.S., Hsu, W.L., Hwang, J.K., and Li, W.H. (2007). Proportion of solvent-exposed amino
634 acids in a protein and rate of protein evolution. Mol. Biol. Evol. *24*, 1005–1011.
635 Lindblad-Toh, K., Garber, M., Zuk, O., Lin, M.F., Parker, B.J., Washietl, S., Kheradpour, P.,
636 Ernst, J., Jordan, G., Mauceli, E., et al. (2011). A high-resolution map of human evolutionary

637 constraint using 29 mammals. Nature *478*, 476–482.
638 Lipman, D.J., Souvorov, A., Koonin, E. V., Panchenko, A.R., and Tatusova, T.A. (2002). The
639 relationship of protein conservation and sequence length. BMC Evol. Biol. *2*, 20.
640 Löytynoja, A. (2014). Phylogeny-aware alignment with PRANK. Methods Mol. Biol. *1079*, 155–
641 170.
642 McBride, C.S. (2007). Rapid evolution of smell and taste receptor genes during host
643 specialization in Drosophila sechellia. Proc. Natl. Acad. Sci. U. S. A.
644 Messer, P.W., and Petrov, D.A. (2013). Frequent adaptation and the McDonald-Kreitman test.
645 Proc. Natl. Acad. Sci. U. S. A. *110*, 8615–8620.
646 Mintseris, J., and Weng, Z. (2005). Structure, function, and evolution of transient and obligate
647 protein-protein interactions. Proc. Natl. Acad. Sci. U. S. A. *102*, 10930–10935.
648 Moutinho, A.F., Trancoso, F.F., Dutheil, J.Y., and Zhang, J. (2019). The Impact of Protein
649 Architecture on Adaptive Evolution. Mol. Biol. Evol. *36*, 2013–2028.
650 Mukherjee, S., and Zhang, Y. (2011). Protein-protein complex structure predictions by
651 multimeric threading and template recombination. Structure *19*, 955–966.
652 Newville, M., Ingargiola, A., Stensitzki, T., and Allen, D.B. (2014). LMFIT: Non-Linear Least-
653 Square Minimization and Curve-Fitting for Python. Zenodo.
654 Nielsen, R., Bustamante, C., Clark, A.G., Glanowski, S., Sackton, T.B., Hubisz, M.J., Fledel-
655 Alon, A., Tanenbaum, D.M., Civello, D., White, T.J., et al. (2005). A scan for positively selected
656 genes in the genomes of humans and chimpanzees. PLoS Biol. *3*, e170.
657 Obbard, D.J., Welch, J.J., Kim, K.-W., and Jiggins, F.M. (2009). Quantifying Adaptive Evolution
658 in the Drosophila Immune System. PLoS Genet. *5*, e1000698.
659 Pál, C., Papp, B., and Hurst, L.D. (2001). Highly expressed genes in yeast evolve slowly.
660 Genetics *158*, 927–931.
661 Palmer, W.H., Hadfield, J.D., and Obbard, D.J. (2018). RNA-interference pathways display high
662 rates of adaptive protein evolution in multiple invertebrates. Genetics *208*, 1585–1599.
663 Pazos, F., and Valencia, A. (2008). Protein co-evolution, co-adaptation and interactions. EMBO
664 J. *27*, 2648–2655.
665 Pieper, U., Webb, B.M., Barkan, D.T., Schneidman-Duhovny, D., Schlessinger, A., Braberg, H.,
666 Yang, Z., Meng, E.C., Pettersen, E.F., Huang, C.C., et al. (2011). ModBase, a database of
667 annotated comparative protein structure models, and associated resources. Nucleic Acids Res.
668 *39*, D465–D474.
669 Ramsey, D.C., Scherrer, M.P., Zhou, T., and Wilke, C.O. (2011). The relationship between
670 relative solvent accessibility and evolutionary rate in protein evolution. Genetics *188*, 479–488.

671 Re, S., Oshima, H., Kasahara, K., Kamiya, M., and Sugita, Y. (2019). Encounter complexes and
672 hidden poses of kinaseinhibitor binding on the free-energy landscape. Proc. Natl. Acad. Sci. U.
673 S. A. *116*, 18404–18409.
674 Sackton, T.B., Lazzaro, B.P., Schlenke, T.A., Evans, J.D., Hultmark, D., and Clark, A.G. (2007).
675 Dynamic evolution of the innate immune system in Drosophila. Nat. Genet. *39*, 1461–1468.
676 Schott, R.K., Refvik, S.P., Hauser, F.E., López-Fernández, H., and Chang, B.S.W. (2014).
677 Divergent positive selection in rhodopsin from lake and riverine cichlid fishes. Mol. Biol. Evol.
678 *31*, 1149–1165.
679 Shao, Y., Chen, C., Shen, H., He, B.Z., Yu, D., Jiang, S., Zhao, S., Gao, Z., Zhu, Z., Chen, X.,
680 et al. (2019). GenTree, an integrated resource for analyzing the evolution and function of
681 primate-specific coding genes. Genome Res. *29*, 682–696.
682 Sironi, M., Cagliani, R., Forni, D., and Clerici, M. (2015). Evolutionary insights into host-
683 pathogen interactions from mammalian sequence data. Nat. Rev. Genet. *16*, 224–236.
684 Slodkowicz, G., and Goldman, N. (2020). Integrated structural and evolutionary analysis reveals
685 common mechanisms underlying adaptive evolution in mammals. Proc. Natl. Acad. Sci. *117*,
686 5977–5986.
687 Smith, N.G.C., and Eyre-Walker, A. (2002). Adaptive protein evolution in Drosophila. Nature.
688 Song, Y., Dimaio, F., Wang, R.Y.R., Kim, D., Miles, C., Brunette, T., Thompson, J., and Baker,
689 D. (2013). High-resolution comparative modeling with RosettaCM. Structure *21*, 1735–1742.
690 Storz, J.F., and Kelly, J.K. (2008). Effects of Spatially Varying Selection on Nucleotide Diversity
691 and Linkage Disequilibrium: Insights From Deer Mouse Globin Genes. Genetics *180*, 367–379.
692 Svetec, N., Cridland, J.M., Zhao, L., and Begun, D.J. (2016). The Adaptive Significance of
693 Natural Genetic Variation in the DNA Damage Response of Drosophila melanogaster. PLoS
694 Genet. *12*, e1005869.
695 Swanson, W.J., Clark, a G., Waldrip-Dail, H.M., Wolfner, M.F., and Aquadro, C.F. (2001).
696 Evolutionary EST analysis identifies rapidly evolving male reproductive proteins in Drosophila.
697 Proc. Natl. Acad. Sci. U. S. A. *98*, 7375–7379.
698 Szklarczyk, D., Gable, A.L., Lyon, D., Junge, A., Wyder, S., Huerta-Cepas, J., Simonovic, M.,
699 Doncheva, N.T., Morris, J.H., Bork, P., et al. (2019). STRING v11: Protein-protein association
700 networks with increased coverage, supporting functional discovery in genome-wide
701 experimental datasets. Nucleic Acids Res. *47*, D607–D613.
702 Tang, C., Iwahara, J., and Clore, G.M. (2006). Visualization of transient encounter complexes in
703 protein-protein association. Nature *444*, 383–386.
704 Thurmond, J., Goodman, J.L., Strelets, V.B., Attrill, H., Gramates, L.S., Marygold, S.J.,

Matthews, B.B., Millburn, G., Antonazzo, G., Trovisco, V., et al. (2019). FlyBase 2.0: The next generation. Nucleic Acids Res. *47*, D759–D765.

Uricchio, L.H., Petrov, D.A., and Enard, D. (2019). Exploiting selection at linked sites to infer the rate and strength of adaptation. Nat. Ecol. Evol. *3*, 977–984.

Uversky, V.N. (2019). Intrinsically Disordered Proteins and Their “Mysterious” (Meta)Physics. Front. Phys. *7*.

Wang, S., Li, W., Liu, S., and Xu, J. (2016). RaptorX-Property: a web server for protein structure property prediction. Nucleic Acids Res. *44*, W430–W435.

Wu, D.D., Wang, G.D., Irwin, D.M., and Zhang, Y.P. (2009). A profound role for the expansion of trypsin-like serine protease family in the evolution of hematophagy in mosquito. Mol. Biol. Evol. *26*, 2333–2341.

Xia, B., Yan, Y., Baron, M., Wagner, F., Barkley, D., Chiodin, M., Kim, S.Y., Keefe, D.L., Alukal, J.P., Boeke, J.D., et al. (2020). Widespread Transcriptional Scanning in the Testis Modulates Gene Evolution Rates. Cell *180*, 248-262.e21.

Yan, J., and Kurgan, L. (2017). DRNApred, fast sequence-based method that accurately predicts and discriminates DNA- and RNA-binding residues. Nucleic Acids Res. *45*, gkx059.

Yanai, I., Benjamin, H., Shmoish, M., Chalifa-Caspi, V., Shklar, M., Ophir, R., Bar-Even, A., Horn-Saban, S., Safran, M., Domany, E., et al. (2005). Genome-wide midrange transcription profiles reveal expression level relationships in human tissue specification. Bioinformatics *21*, 650–659.

Yang, Z. (2007). PAML 4: Phylogenetic analysis by maximum likelihood. Mol. Biol. Evol. *24*, 1586–1591.

Yang, L., Zhang, Z., and He, S. (2016). Both Male-Biased and Female-Biased Genes Evolve Faster in Fish Genomes. Genome Biol. Evol. *8*, 3433–3445.

Yang, Z., Wong, W.S.W., and Nielsen, R. (2005). Bayes empirical Bayes inference of amino acid sites under positive selection. Mol. Biol. Evol. *22*, 1107–1118.

Zhang, J., and He, X. (2005). Significant impact of protein dispensability on the instantaneous rate of protein evolution. Mol. Biol. Evol. *22*, 1147–1155.

Zhang, J., and Yang, J.R. (2015). Determinants of the rate of protein sequence evolution. Nat. Rev. Genet. *16*, 409–420.

Zhang, Y.E., Vibranovski, M.D., Krinsky, B.H., and Long, M. (2010). Age-dependent chromosomal distribution of male-biased genes in Drosophila. Genome Res. *20*, 1526–1533.

Zheng, N., Schulman, B.A., Song, L., Miller, J.J., Jeffrey, P.D., Wang, P., Chu, C., Koepp, D.M., Elledge, S.J., Pagano, M., et al. (2002). Structure of the Cul1-Rbx1-Skp1-F boxSkp2 SCF

ubiquitin ligase complex. Nature *416*, 703–709.

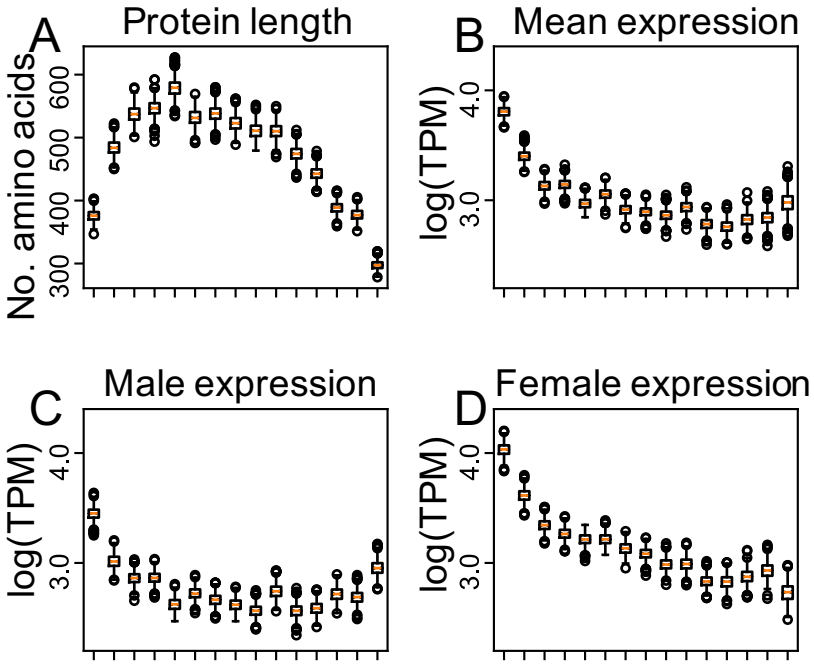


**Figure 1**. Protein length (A), mean (B), male (C) and female expression (D) levels in each gene groups divided by ascending $\omega$ values. Values for each gene group and each gene property were computed through 1,000 bootstrapping steps. Obvious complex U-shaped correlations with $\omega$ were observed for protein length (A) and male expression level (C).

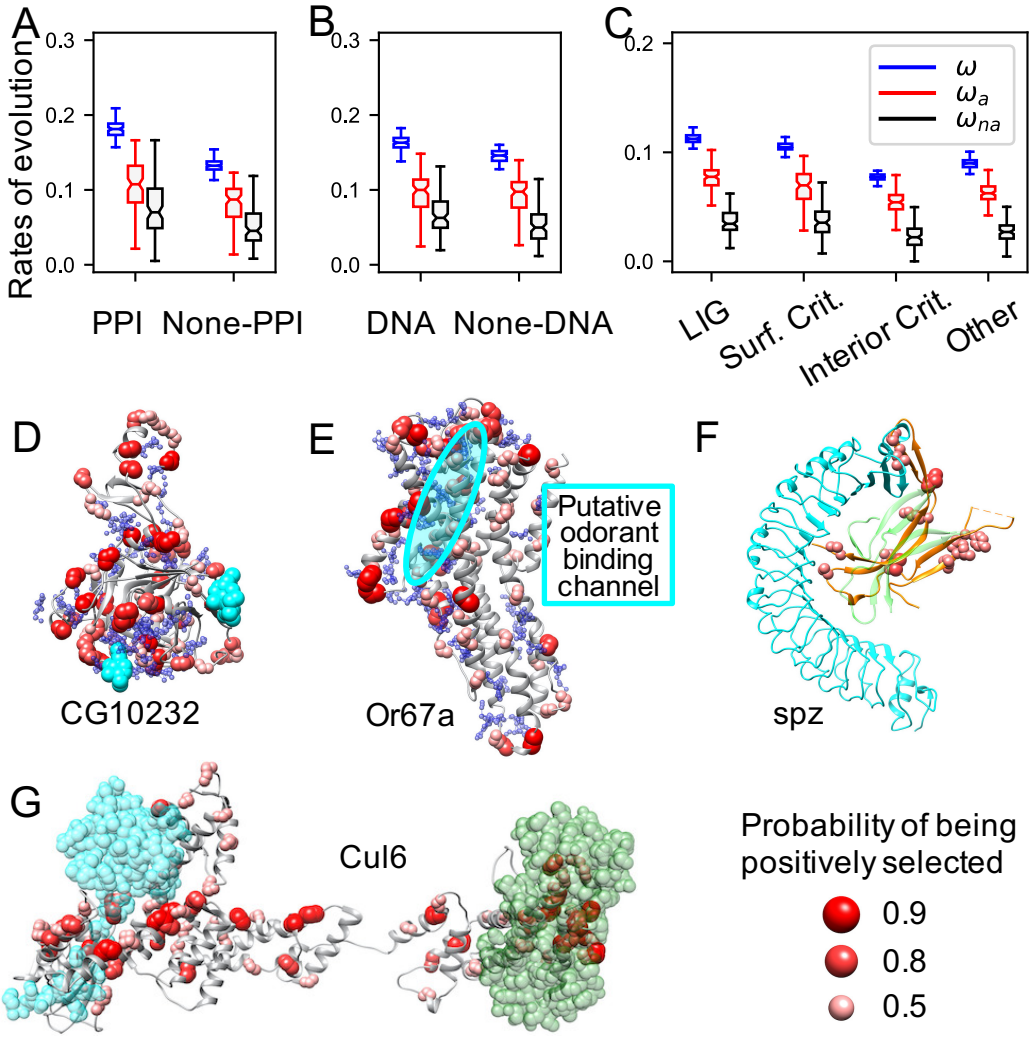


Figure 2. Adaptive evolution in molecular interaction sites. Protein-protein interaction sites (A), DNA binding sites (B) and putative ligand binding sites (C) show higher adaptation rates than none binding sites. Examples of positive selection around molecular interaction sites in high quality structural models of CG10232 (D), Or67a (E), spz (F), and Cul6 (G). Except for spz (PDB code 3e07), the other proteins are obtained from SWISS model repository. Putative ligand binding pockets of CG10232 (D) and Or67a (E) are shown in blue spheres. Ligands including interacting proteins are shown in cyan or green: NAG of CG10232 in cyan (D), Toll receptor of spz in cyan (F), RING-box protein in cyan and F-box protein in green for Cul6 (G). The putative odorant binding channel of Or67a is highlighted in cyan circle (E). The ligand poses in (D, F and G) are obtained by superimposition from structure 2XXL, 4BV4 and 1LDK, respectively.

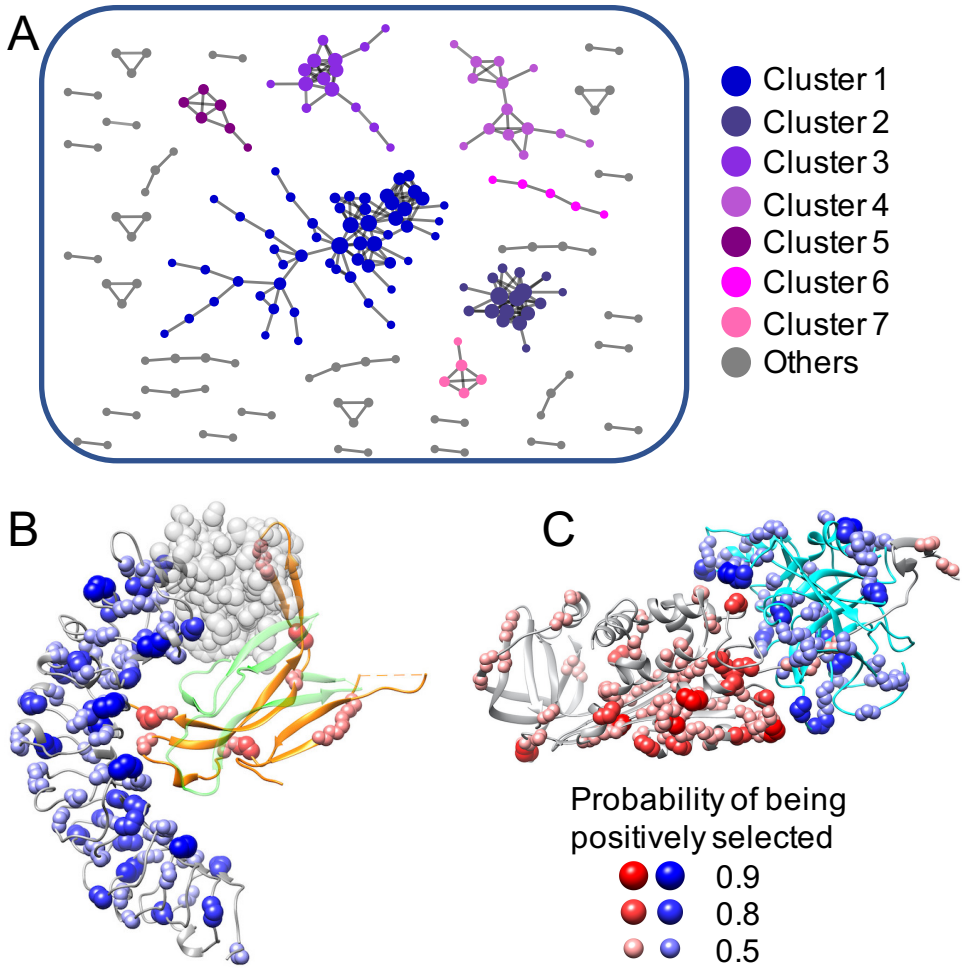


Figure 3. Co-adaptation of fast-adaptive proteins. (A) Sub-clusters of PPI networks of fast-adaptive proteins. Only proteins with at least one partner were shown. Examples of molecular interactions that might regulate co-adaptation in fast-adaptive proteins: (B) Toll-4 (gray) and spz (orange, with green representing the other spz monomer), (C) Spn28Db (gray, serine protease inhibitor 28Db) and CG18563 (cyan, with Go term “serine-type endopeptidase activity”). A putative N-terminus (transparent beads) of Toll-4 were built by superimposition from 4LXR, since the N-terminus were missing in the structural model. Complex structural model of Spn28Db and CG18563 was inferred from 1EZX.

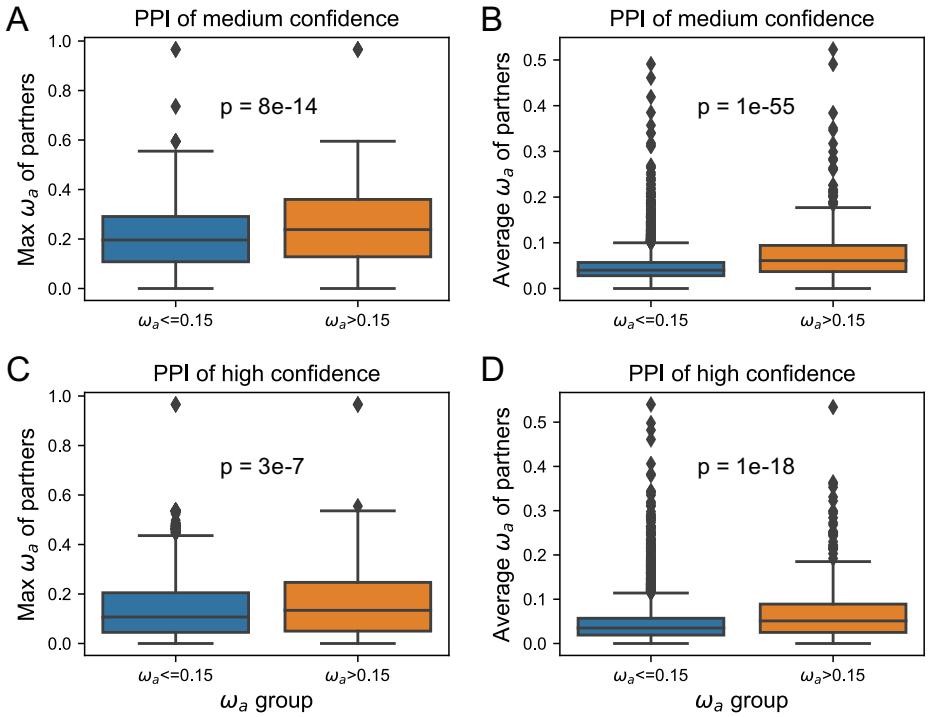


Figure 4. Co-adaptation of PPIs in *D. melanogaster*. For fast-adaptive proteins, adaptation rates of their partners (orange box plot) are significantly larger compared to slow adaptive proteins (blue box plot). Max $\omega_a$ of protein partners are shown in (A and C) and averaged $\omega_a$, of protein partners are shown in (B and D). PPI from STRING with median confidence (combined score larger than 0.4) are shown in (A and B), and PPI with high confidence (combined score larger than 0.7) are shown in (C and D).

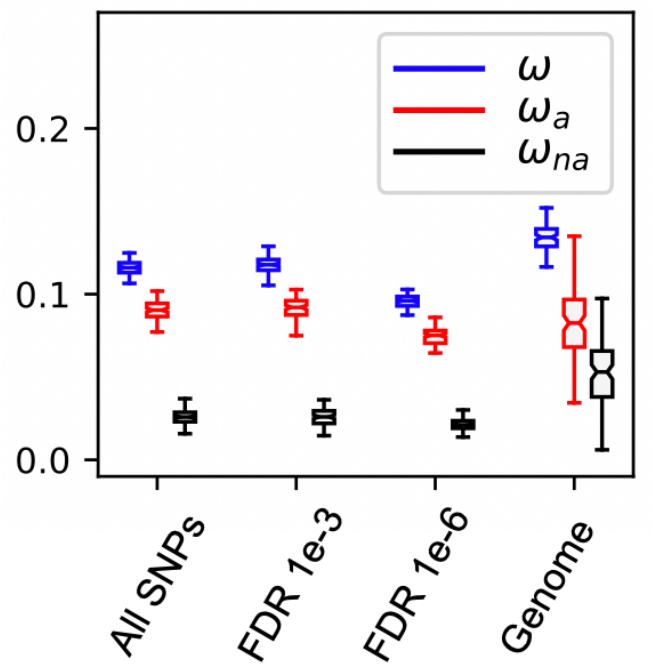


Figure 5. Adaptive evolution in FST SNPs. The significant SNPs at different FDR cutoffs all show much higher proportions of adaptation than genome-wide expectation.

**Table 1.** Pearson correlation coefficients between ω, $\omega_a$ and $\omega_{na}$ and gene properties [a]

| Categories | Properties | ω | | $\omega_a$ | | $\omega_{na}$ | |
|---|---|---|---|---|---|---|---|
| Function-related properties | Gene age | 0.55 | (0) | 0.34 | (7e-154) | 0.41 | (2e-224) |
| | Protein length [b] | -0.22 | (2e-136) | -0.13 | (1e-25) | -0.30 | (2e-142) |
| | Mean expression [b] | -0.21 | (2e-109) | -0.11 | (2e-18) | -0.11 | (1e-18) |
| | Male expression [b] | -0.06 | (5e-10) | 0.00 | (8e-1) | -0.03 | (6e-2) |
| | Female expression [b] | -0.29 | (2e-205) | -0.17 | (2e-42) | -0.16 | (3e-35) |
| | Male specificity | 0.21 | (2e-104) | 0.12 | (3e-22) | 0.10 | (3e-14) |
| | Tissue Specificity | 0.30 | (4e-226) | 0.18 | (1e-45) | 0.19 | (3e-48) |
| | PPI number [b] | -0.28 | (1e-217) | -0.14 | (4e-29) | -0.19 | (4e-58) |
| | PPI-site ratio | 0.14 | (1e-50) | 0.05 | (7e-6) | 0.10 | (2e-16) |
| | DNA-site ratio | 0.25 | (8e-164) | 0.12 | (3e-23) | 0.23 | (3e-79) |
| Structure-related properties | Helix ratio | -0.05 | (4e-7) | -0.01 | (3e-1) | -0.05 | (4e-5) |
| | Sheet ratio | -0.04 | (2e-5) | 0.00 | (9e-1) | -0.01 | (3e-1) |
| | Helix+sheet ratio | -0.09 | (3e-25) | -0.02 | (1e-1) | -0.07 | (1e-9) |
| | Coil ratio | 0.10 | (8e-27) | 0.01 | (2e-1) | 0.08 | (8e-11) |
| | ISD | 0.17 | (8e-82) | 0.04 | (1e-3) | 0.12 | (2e-24) |
| | RSA | 0.16 | (7e-87) | 0.06 | (1e-6) | 0.15 | (3e-35) |
| Protein evolution | ω | 1.00 | (0) | 0.65 | (0) | 0.78 | (0) |
| | $\omega_a$ | 0.65 | (0) | 1.00 | (0) | 0.03 | (7e-3) |
| | $\omega_{na}$ | 0.78 | (0) | 0.03 | (7e-3) | 1.00 | (0) |

[a] Pearson correlation coefficient R were listed along with corresponding P-values in parentheses.

790 [b] To better estimate the correlations for sequence length, expression levels and PPI numbers,
791 we used logarithmic scales rather than absolute values, which could vary dramatically from near
792 zero to thousands.
793 Abbreviations in this table: ISD, intrinsic structural disorder; RSA, relative solvent accessibility;
794 PPI number, protein-protein interaction number; PPI-site ratio, ratio of protein-protein interaction
795 sites; DNA-site ratio, ratio of DNA-binding sites.
796